https://dx.doi.org/10.21577/0103-5053.20230025

J. Braz. Chem. Soc., Vol. 34, No. 8, 1119-1129, 2023

Article

Mechanism and Kinetics of the Degradation of Nitazoxanide and Hydroxychloroquine Drugs by Hydroxyl Radicals: Theoretical Approach to Ecotoxicity

Flávio O. Sanches-Neto,[a] Nayara D. Coutinho,[,b] Vincenzo Aquilanti,[c,d] Wender A. Silva[b] and Valter H. Carvalho-Silva[*,a,e]*

[a]*Instituto de Química, Universidade de Brasília, CP 4478, 70904-970 Brasília-DF, Brazil*

[b]*Laboratório de Planejamento e Síntese de Compostos Ativos, Universidade de Brasília (IQ-UnB), Campus Universitário Darcy Ribeiro, 70904-970 Brasília-DF, Brazil*

[c]*Dipartimento di Chimica, Biologia e Biotecnologie, Università di Perugia, 06123 Perugia, Italy*

[d]*Istituto di Struttura della Materia, Consiglio Nazionale delle Ricerche, 00133 Rome, Italy*

[e]*Laboratório de Modelagem de Transformações Físicas e Químicas, Universidade Estadual de Goiás, 75132-903 Anápolis-GO, Brazil*

The efforts of contrasting the effects caused by the COVID-19 (coronavirus disease 2019) pandemic increased the disposal of active pharmaceutical ingredients. This paper reports the mechanisms and kinetics of the degradation in aqueous environments induced by •OH of two drugs, among those most widely probed at the outbreak of coronavirus, nitazoxanide and hydroxychloroquine. The investigation exploits quantum chemistry techniques and a reaction rate theory combined with diffusion-controlled processes and quantum mechanical tunneling. The reaction rate constants are obtained in an environmentally relevant temperature range. The results show that (*i*) the deacetylation of nitazoxanide with formation of tizoxanide is kinetically the most favorable channel, in agreement with experimental work; (*ii*) for hydroxychloroquine, the present theoretical calculations show that the most favorable channel is the addition of •OH at the aromatic ring. The half-life time degradation products are for both cases in the range between 12 to 138 days. Both drugs presented toxicities between harmful and toxic as obtained by computational toxicology calculations. The toxicity is also calculated for the degradation products: (*i*) in the nitazoxanide degradation process, tizoxanide was characterized as more toxic, while (*ii*) in the case of hydroxychloroquine, the major degradation product showed a decrease in the toxicity.

Keywords: APIs, oxidative degradation process, nitazoxanide, hydroxychloroquine, COVID-19

Introduction

In recent years, the occurrence of micropollutants, such as those originated from waste of pharmaceuticals and pesticides, has turned into a global environmental concern.[1,2] The COVID-19 (coronavirus disease 2019) pandemic worsened this scenario, since the effort to control the adverse health effects caused by the disease increased the variety and the quantities of pharmaceuticals in surface waters and sewage.[3,4] Persistent and excessive use makes the metabolization of these drugs incomplete within the human body and a significant fraction are excreted by the organism of patients through their feces and urines, which will end up in sewage.[5]

When active pharmaceutical ingredients (APIs) are dispersed in the environment, they become threats to aquatic wildlife, being often associated with several negative effects, e.g., disruption of cellular processes, intracellular ion concentrations, antibiotic resistance of microorganisms and the bio-accumulation of pharmaceuticals.[6] Furthermore, these pharmaceuticals represent a potential danger to human health since a lot of reports have been confirmed their persistence in water bodies, oceans, groundwater, and even in the drinking water of several countries around the world.[5,7]

Conventional widely used urban wastewater treatment plants, either primary (physical and physicochemical)

*e-mail: nayaradcoutinho@gmail.com; fatioleg@gmail.com
Editor handled this article: Paula Homem-de-Mello (Associate)

or secondary (biological), are inefficient to remove APIs.[8] Over the past decades, many efforts have been allocated in the development of new technologies as an alternative to wastewater treatment plants that can eliminate pharmaceuticals from wastewater, such as granular activated carbon,[9] membrane filtration,[10] and AOP, advanced oxidation processes.[11,12] Researchers have been pointing out the AOP as one of the most effective and versatile advanced water treatments.

This method is based on the generations of a powerful oxidizing agent, such as the hydroxyl radical (•OH) in solution, which is then able to degrade recalcitrant organic pollutants up less harmful compounds or even completely mineralize to CO_2 and H_2O.[13] This method has gained increasing attention in studies of the removal of pharmaceuticals involving fast reaction rates and strong oxidation capability.[12,14,15] Typical AOPs (Fenton, ozonation, photocatalytic oxidation, and electrooxidation) have been used for the removal of different kinds of drugs from water or wastewater (for instance, ibuprofen,[16-18] carbamazepine,[16,19-21] amoxicillin,[22-24] sulfamethoxazole,[25-28] and paracetamol).[29-32]

The reactive elementary steps for mitigation of micropollutants by •OH radicals evolve primarily along three paths:[32-35] addition of •OH to an aromatic ring or to other unsaturated bonds, hydrogen-atom transfer (HAT), and single electron transfer (SET). The identification and elucidation of the degradation mechanisms from experimental techniques are complex, equipment-dependent and expensive.[34-36] These arduous experimental procedures provide a detailed investigation of the real network and an assessment of the involved reaction kinetics.[37-40]

As soon as the SARS-COV-2 pandemic emerged, there has been a huge number of reports from all over the world proposing options for treatments of the disease and also for preventive therapy. Today we have some drugs indicated for use in specific conditions of COVID-19, such as monoclonal and antiviral antibodies,[41,42] in parallel keep going investigations for the development of effective vaccines. However, large quantities of drugs such as chloroquine/hydroxychloroquine, lopinavir/ritonavir, azithromycin, nitazoxanide, and colchicine have been produced for testing, and also prescribed by doctors to patients worldwide, even with several studies indicating ineffectiveness against COVID-19.[1,43,44] Their fate and removal represent a relevant environmental worldwide concern. In this study, we focus from a theoretical point of view on the degradation mediated by •OH radicals of two of those drugs, nitazoxanide and hydroxychloroquine, that have been widely produced and distributed, especially in Brazil.

Nitazoxanide (NTZ) belongs to the class of drugs known as thiazolides, which has broad-spectrum antiparasitic and antiviral properties.[45] Very recently, a multicenter, randomized, double-blind, placebo-controlled study involving COVID-19 patients,[46] showed that five days of NTZ treatment did not accelerate symptom resolution but reduced the viral load compared to the placebo group with no serious adverse events.[46] Specifically, this study has some methodological flaws that will not be discussed in this work. Stress degradation study[47] of raw material and NTZ showed that the major degradation product is tizoxanide (2-hydroxy-*N*-(5-nitro-2-thiazolyl)benzamide) originated from its deacetylation for all tested stress conditions (thermal, acid, alkaline and oxidative).

Hydroxychloroquine (HQC) belongs to the group of 4-aminoquinolines that has been used in the treatment of malarial and rheumatology diseases.[48-50] Recently, it has been used in the treatment of COVID-19, but until the time of this paper, several articles showed that there is no support for its use against COVID-19.[51-53] The nitrogenous heterocyclic quinolone increases hydrophilicity which rising the persistence of HCQ that bioaccumulate in the environment. Investigations of fate and degradation of HCQ in aqueous environment are rare and concentrate specifically on the photochemical degradation of HCQ in water solution.[54,55] Bensalah *et al*.[56] recently presented a study of the degradation of HCQ in water solution by elaborated electrochemical involving oxidation treatment including boron doped diamond combined with sonication and UV irradiation. It was demonstrated that release of chloride ions at the first stages of degradation of HCQ, followed by conversion of organic nitrogen compounds into NO_3^- and NH_4^+, confirming the formation of 7-chloro-4-quinolinamine, oxamic and oxalic acids as final products of HCQ degradation by electrochemical oxidation.

Thus, the focus of this work is to provide a detailed understanding of the mechanism and kinetics of nitazoxanide and hydroxychloroquine degradation mediated by •OH radicals using a combination of quantum chemistry calculations and reaction rate theory. In addition, we provide the toxicity of nitazoxanide and hydroxychloroquine and of their main degradation products from Ecological Structure-Activity Relationships predictive model. As far as we are aware, of the two most common mechanisms, radical adduct formation to the carbon (RAF) and hydrogen atom transfer (HAT) reactions involving •OH are the major steps for mitigation of contaminants because the energetic barrier involved in SET reactions are much higher,[38,39,57] and consequently it is of no concern here.

Methodology

Quantum chemical calculations of properties of reactants, products, and transition states

To identify the most reactive sites of the APIs (NTZ and HCQ) with the •OH radical, appropriate local reactivity descriptors, such as the Fukui function (*f*)[58,59] were calculated according to equations $f^{+} = \sum_{i} |c_i|^2_{HOMO}$, $f^{-} = \sum_{i} |c_i|^2_{HOMO}$, and $f^{0} \approx \left(f^{+} + f^{-}\right)$. It was used Multiwfn package program,[60] where the contributions of the atomic orbitals of the frontier molecular orbital are weighted by the c_i coefficients of highest occupied molecular orbital (HOMO) and lowest unoccupied molecular orbital (LUMO) orbitals.

All the quantum chemical calculations were carried out using the Gaussian 16 package.[61] The electronic structure properties of the reactants, products, and the transition states of the degradation channels of the pharmaceutical compounds (NTZ and HCQ) by •OH radicals were calculated at the MP2/6-31+G//M06HF/6-31G(d) level of calculation, including the SMD version of the Continuum Solvation Model[62] to simulate the aqueous environment. The stationary points were characterized by analytical harmonic frequency analysis of the optimized structures, no imaginary frequency individuating local minima, one imaginary frequency individuating transition states. The zero-point vibrational energy contributions have been considered in the calculation of the energy barrier.

Reaction rate theory

The reaction rate constants of the degradation of the pharmaceuticals compounds (HCQ and NTZ) by •OH radicals were calculated using a combination of formulations derived from the Transition State Theory. To account for the tunneling effect, the deformed Transition State Theory (d-TST)[63] was adopted (equation 1):

$$k_{d-TST} = \frac{k_B T}{h} \frac{Q_{TS^{\ddagger}}}{Q_{Reac}} \left(1 - d\frac{E_0}{RT}\right)^{1/d} \quad (1)$$

where h is the Planck's constant, k_B is the Boltzmann constant, R is the universal gas constant, *d* is the deformation parameter, while Q_{Reac} and $Q_{TS^{\ddagger}}$ are the partition functions of the reactants and transition state, respectively. To include the contribution of molecular diffusion in solution, the calculated rate constant k_{d-TST} is combined with the Smoluchowski rate constant, k_D, following the steady-state suggestion by Collins and Kimball,[64] yielding the overall rate constant k_{OBS}, according to equation 2:

$$\frac{1}{k_{OBS}} = \frac{1}{k_{d-TST}} + \frac{1}{k_D} \quad (2)$$

Additional details about the parameter *d* and the calculation of k_D can be found elsewhere[65] and the references therein. The overall reaction rate constant for the Ri channel were used to calculate the total reaction rate constant $k_{Total} = \sum_{i} k_{Ri}$. The Aquilanti-Mundim formula[66] (equation 3) was used to represent the temperature dependence our results for $k_{Total}(T)$ for comparison with other works and for use in kinetic models.

$$k_{Total} = A\left(1 - \frac{\bar{d}\bar{E}}{RT}\right)^{1/\bar{d}} \quad (3)$$

where *A* and $\bar{d}$ are the pre-exponential factor and the deformation parameter, respectively. Note a change in the notation here, needed in order to avoid ambiguities: in general, the parameters $\bar{d}$ and $\bar{E}$ from the fitting equation 3 can differ from the *d* and E_0 parameter in equation 1. Equation 3 permits to evaluate prototypical systems where the temperature dependence of the rate constant according to this equation is described by $\bar{E} > 0$ and $\bar{d} > 0$ or $\bar{d} < 0$, corresponding to convex (Super-Arrhenius) and concave (sub-Arrhenius). In the limit $\bar{d} \longrightarrow 0$, the term $\left(1 - \frac{\bar{d}\bar{E}}{RT}\right)^{1/\bar{d}}$ can be identified with the Arrhenius exponential law. Other case for $\bar{E} < 0$ will also be documented and indicated as anti-Arrhenius.

All kinetic and associated parameters have been calculated with the Transitivity Code version 1.0.4.[67] Details of the computational program can be found on the literature.[68]

Assessment of toxicity

The ecotoxicity of NTZ and HCQ and its main degradation products were determined using the Ecological Structure-Activity Relationship Model (ECOSAR V2.0).[69] ECOSAR is an effective predictive program and has been successfully applied to the ecotoxicity assessment of organic contaminants.[70,71] Three aquatic organisms (green algae, daphnia, and fish) were chosen as targets. Acute toxicity (feature characterized by LC_{50} and EC_{50} values) and chronic toxicity (defined by ChV) of the compounds studied were obtained from ECOSAR platform. LC_{50} means the concentration of a chemical compound (in mgL^{-1}) that causes the death of half of the fish and daphnia population after exposures of 96 and 48 h, respectively. In addition, EC_{50} represents the concentration that permits 50% of green algae to grow normally after 96 h of exposure (in mg L^{-1}).

Results and Discussion

The results of the present study can help understanding the mechanism and kinetic of reactions of nitazoxanide and hydroxychloroquine with •OH, also providing relevant clues on risk assessment in aqueous environments. Fukui functions are descriptors that allow the identification of the most reactive sites on a molecule, both for electrophilic as for nucleophilic and radical reactions.[72] Here, f^0 parameters identify the most important reactive sites on NTZ and HCQ under •OH attack.[36,58,59,73] The relevant values of the Fukui function are shown in Figures S1 and S2 in Supplementary Information (SI) section for the selected atoms.

Nitazoxanide

The nomenclature and main mechanism of hydrogen atom abstraction and addition reaction of NTZ and •OH radicals are shown in Figure 1: (*i*) hydrogen atom transfer (HAT) from carbon (R1, R2, and R4) or nitrogen (R3) of NTZ to the •OH radical and (*ii*) •OH addition (RAF) to the carbon of the NTZ (R5 and R6).

Figure 1 shows the energetic kinetic and thermodynamic parameters of the reaction of NTZ with •OH radicals showing that R1, R5 and R6 channels are thermodynamically favorable (free energy $\Delta G° < 0$) (while R5 channel shows the lowest barrier heights (reaction barrier energies (E_0) = –3.55 kcal mol^{-1}), indicating that R5 is the most kinetically favorable channel and tizoxanide (2-hydroxy-*N*-(5-nitro-2-thiazolyl)benzamide) is the majority degradation product: this agrees with previous experimental results.[51]

Here, it is worth noting that the rate of some process increase as temperature decreases accordingly to an apparently negative activation energy. These processes are classified as anti-Arrhenius. In gas-phase reactions the anti-Arrhenius behavior is often found in molecule-radical reactions.[74-78] An interpretation of negative dependence of the rate constant on temperature for OH + HBr and OH + HI reactions was provided using first principle Born-Oppenheimer molecular dynamics.[79-81] The simulations confirmed the suggestion obtained experimentally: the stereodynamical effect arises at low temperature permitting, the reactants reorient to find the propitious alignment leading to reaction; however, this adjustment is progressively less effective for higher temperatures, where the wandering paths evidence the roaming effect.

The Cartesian coordinates of the transition states and NTZ calculated in this work are listed in Table S1 (SI section). Geometric parameters and imaginary frequencies of the transition states involved in the reaction of •OH radicals with NTZ are listed in Table S2 (SI section). For the transition state of the R5 channel, we found the values 97.76° for $C_5–O_7–H_8$ angle, the imaginary frequency of 525 cm^{-1}, energy barrier E_0 = –3.55 kcal mol^{-1} and deformation parameter d = –0.0149.

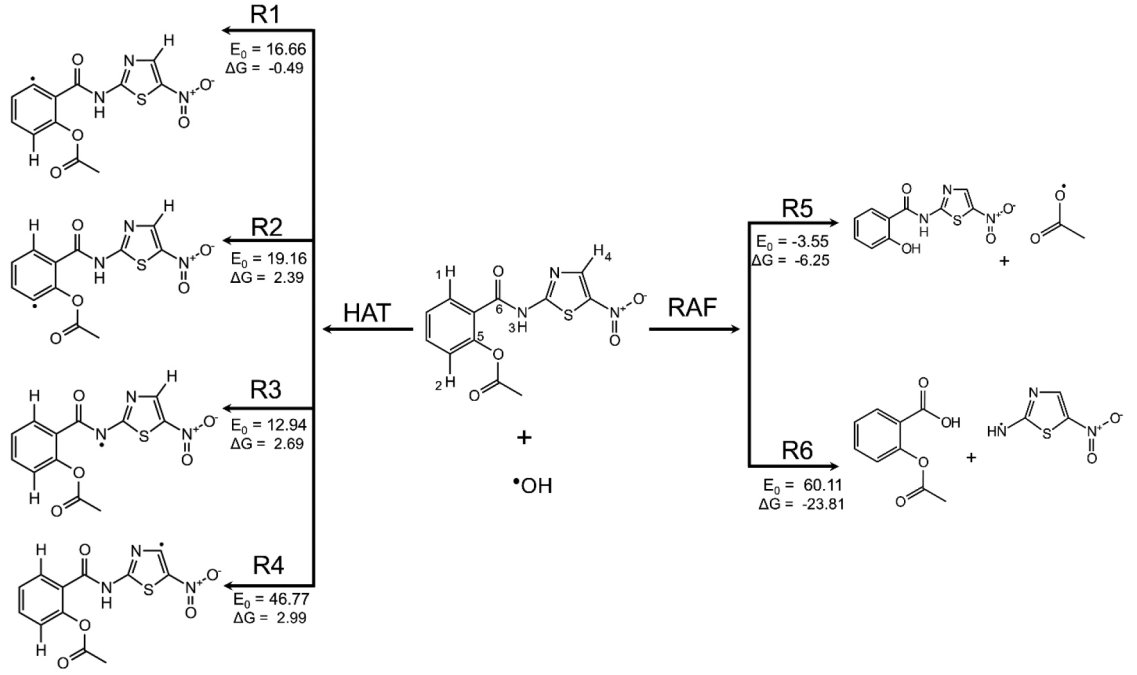

Figure 1. Scheme of hydrogen atom abstraction (HAT) and addition reactions (RAF) with nitazoxanide and •OH radical. Reaction barrier energies (E_0) and free energies (ΔG) in kcal mol^{-1} were calculated at the MP2/6-31+G//M06HF/6-31G(d) level of theory.

Reaction rate constants

Reaction rate constants are key quantities for evaluating the efficiency of the kinetics for degradation of drugs[80] permitting to quantify the relevance of the alternative reactive paths for the global conversion of each compound. Inclusion of molecular diffusion in solution is performed by the combination of the rate constant k_{d-TST} and the steady-state Smoluchowski rate constant k_D, according to the Collins-Kimball theory at 250-310 K (see equation 2 and results in Table 1). Our calculations provided values of the total reaction rate constant around 5.82×10^{12} cm^3 mol^{-1} s^{-1} at 298.15 K, however, the comparison with experimental data is impeditive since there is no known data. The reaction rate constant are much larger than the overall reaction rate constants (see Table S3, SI section), reporting diffusion-controlled processes.

Web applications recently developed by our group used machine learning and a molecular fingerprint algorithm to evaluate the reaction rate constants for the degradation of contaminants in aqueous and atmospheric environments (the pySiRC platform).[81,82] The reaction rate constant calculated by the Random Forest Machine Learning model in pySiRC platform demonstrated an excellent agreement with high-level reaction rate constant calculated with a value of 5.04×10^{12} cm^3 mol^{-1} s^{-1}. The CAS-numbers used for NTZ and HCQ are 55981-09-4 and 118-42-3, respectively.

To evaluate the total reaction rate constant of NTZ with •OH radicals, we fitted the temperature dependence using the Aquilanti-Mundim (AM) formula (equation 3), which has been used successfully to describe the temperature dependence k of chemical processes under condition from Non-Arrhenius behavior.[78] The equation obtained from fit for the overall rate constant is expressed as:

$$k_{Total} = 1.2610^{-8}\ cm^3\ molecules^{-1}\ s^{-1}\left(1-\frac{65.40}{T}\right)^{29.07} \quad (4)$$

The phenomenological parameters obtained from the fit by the AM formula were $\bar{E}$ = 3.764 kcal mol^{-1} and $\bar{d}$ = 0.0344. Positive values of these parameters are characteristic of the super-Arrhenius behavior of the viscosity of the solvent involved in the reaction.

From the data of the total reaction rate constant of NTZ with the •OH radical, it is possible to calculate the half-life time using $t_{1/2} = \ln 2/(k_{Total} \times [\bullet OH])$, where [•OH] is the concentration of •OH radicals in the specific aqueous medium. The half-life of the reaction was studied by us in the temperature range 273.15-310 K, using [•OH] = 10^{-15}-10^{-18} mol L^{-1}, which usually represents values typical of surface waters. The calculated half-lives are shown in Figure 2 and they vary from 14 to 138 days at 298.15 K, considering a concentration of •OH radicals in the restricted range 10^{-16}-10^{-17} mol L^{-1}.

Hydroxychloroquine

Based on Fukui functions, we proposed seven degradation channels by •OH attack in the neutral form of HCQ. The nomenclature is shown in Figure 3 being: (*i*) •OH addition to the carbon (RAF) of the HCQ (R1-R4); (*ii*) hydrogen transfer from carbon (HAT) of HCQ to the •OH radical (R5-R7).

The calculated energy parameters of the reaction of HCQ with •OH radicals show that, with the exception of R6, all other channels are thermodynamically favorable ($\Delta G° < 0$), wherein R2 is the most favorable one ($\Delta G° = -19.01$ kcal mol^{-1}), while the R6 channel shows the lowest barrier height ($E_0 = -18.86$ kacl mol^{-1}). The Cartesian coordinates and imaginary frequencies of the transition states and HCQ calculated in this work are listed in Tables S4 and S5 (SI section).

Table 1. Reaction rate constants of NTZ degradation by •OH attack calculated at the MP2/6-31+G//M06HF/6-31G(d) level with the SMD continuous solvation model using d-TST formulation combined with the steady-state Smoluchowski rate constant

	Rate constant (k) / (cm^3 mol^{-1} s^{-1})				
Temperature / K	273.15	298.15	300.0	310.0	320.0
k_{R1}	1.10×10^{1}	6.81×10^{1}	7.71×10^{1}	1.48×10^{2}	2.75×10^{1}
k_{R2}	4.80×10^{-1}	4.69×10^{-1}	5.47×10^{-1}	1.23×10^{0}	2.65×10^{0}
k_{R3}	3.43×10^{3}	1.36×10^{4}	1.49×10^{4}	2.44×10^{4}	3.90×10^{4}
k_{R4}	6.00×10^{-24}	3.79×10^{-21}	5.87×10^{-21}	5.72×10^{-20}	4.87×10^{-19}
k_{R5}	2.61×10^{12}	5.82×10^{12}	6.10×10^{12}	7.7×10^{12}	9.59×10^{12}
k_{R6}	1.03×10^{-36}	8.98×10^{-33}	1.66×10^{-32}	3.99×10^{-31}	7.91×10^{-30}
$k_{Total} = \sum_{i}^{6} k_{Ri}$	2.61×10^{12}	5.82×10^{12}	6.10×10^{12}	7.7×10^{12}	9.59×10^{12}

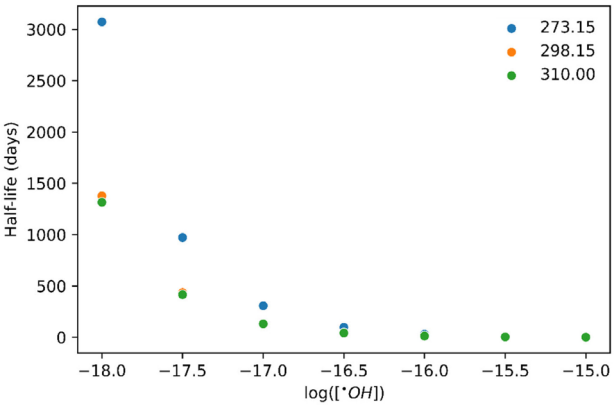

Figure 2. Half-life time, in days, of nitazoxanide degradation as a function of •OH concentration, in mol L^{-1}, in the temperature range 273.15-310 K of interest in natural waters.

Reaction rate constant

The reaction rate constants for all seven channels were combined with the Collins-Kimball formulation in the relevant temperature range 250.0-310.0 K to elucidate the most important products of degradation. The results are presented in Table 2. The R2 channel was found to have the fastest reaction rate constant, and its product is most kinetically favorable by •OH attack in HCQ. The value of the total reaction rate constant at 298.15 K is 6.64×10^{12} cm^3 mol^{-1} s^{-1}, however, there are no experimental reaction rate constants in the same theoretical conditions simulated and consequently, these results and the mechanism proposed here can be confronted with future experimental results. For R2 channel, we found the values E_0 = –4.21 kcal mol^{-1} for energy barrier and d = –0.1642 for deformed parameter.

As observed for NTZ, the reaction rate constant for HCQ showed a diffusion-controlled process (see Table S6, SI section). The reaction rate constant estimated by the random forest machine learning (ML) model in pySiRC showed a value of 6.09×10^{12} cm^3 mol^{-1} s^{-1}, which showed a good agreement with high-level reaction rate constant calculation. The fitting of temperature dependence of the rate constant using AM formula is expressed as:

$$k_{Total} = 9.1510^{-9}\ cm^3\ molecules^{-1}\ s^{-1}\left(1-\frac{66.76}{T}\right)^{26.61} \quad (5)$$

The phenomenological parameters obtained from the fit by the AM formula were $\bar{E}$ = 3.517 kcal mol^{-1} and $\bar{d}$ = 0.0376. Similarly to kinetic behavior observed for the NTZ drug, here the parameters also presented positive values, which are related with super-Arrhenius behavior.

In an advanced oxidative experimental study, Lu and Chen[60] evidenced the formation of the CQLA (7-chloro-4-quinolinamine) as one of the most important intermediate degradant products, however, in their experimental conditions, two of the functional groups exist in protonated forms, which may facilitate the rupture of C–N bonds by •OH radical attack.

The half-life of the reaction was studied by us in the temperature range 273.15-310 K, using [•OH] = 10^{-15}-10^{-18} mol L^{-1}, which usually represents values typical of surface waters.[83-85] The calculated half-lives are shown in Figure 4, and they vary from 12 to 121 days at 298.15 K, considering a concentration of •OH radicals in the restricted range 10^{-16}-10^{-17} mol L^{-1}.

Evaluation of toxicity

Table 3 exploit discrimination criteria established by the European Union[86] and Chinese Regulations[87] for

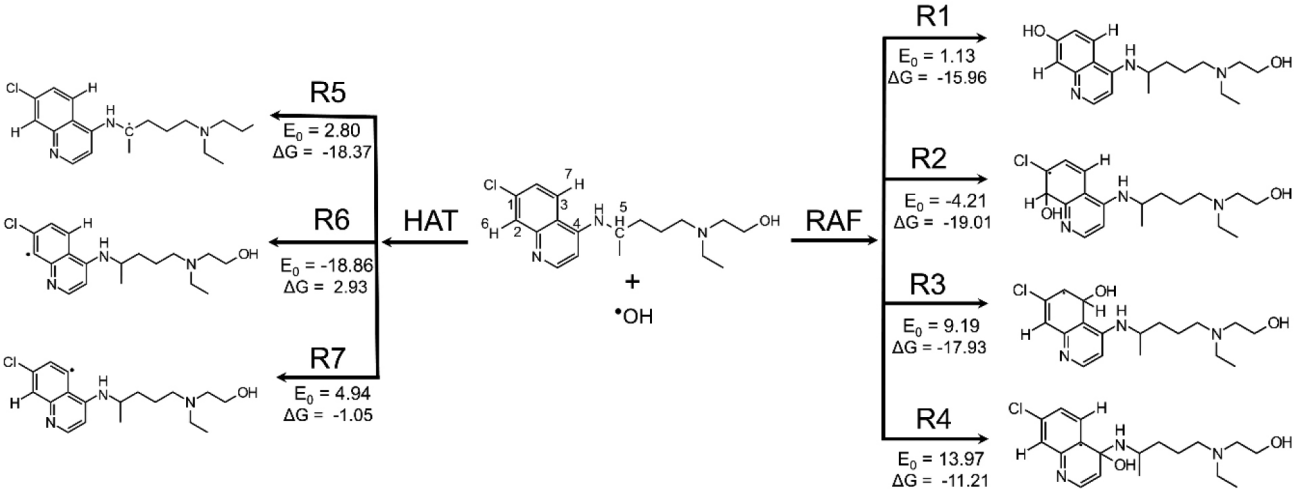

Figure 3. Scheme of hydrogen atom abstraction and addition reactions with HCQ and •OH radical. Reaction barrier energies (E_0) and free energies (ΔG) in kcal mol^{-1} were calculated at the MP2/6-31+G//M06HF/6-31G(d) level of theory.

Table 2. Reaction rate constants of HCQ degradation by •OH attack calculated at the MP2/6-31+G//M06HF/6-31G(d) level with the SMD continuous solvation model using Collins-Kimball formulation

	Rate constant (k) / (cm^3 mol^{-1} s^{-1})				
Temperature / K	273.15	298.15	300.0	310.0	320.0
k_{R1}	1.85×10^{11}	1.95×10^{11}	1.96×10^{11}	1.98×10^{11}	2.00×10^{11}
k_{R2}	2.88×10^{12}	6.39×10^{12}	6.69×10^{12}	8.46×10^{12}	1.04×10^{12}
k_{R3}	3.10×10^{5}	1.17×10^{6}	1.28×10^{6}	2.03×10^{6}	3.14×10^{6}
k_{R4}	5.03×10^{1}	3.82×10^{2}	4.38×10^{2}	8.89×10^{2}	1.73×10^{3}
k_{R5}	4.75×10^{10}	5.77×10^{10}	5.85×10^{10}	6.27×10^{10}	6.71×10^{10}
k_{R6}	5.44×10^{-3}	5.61×10^{-2}	6.57×10^{-2}	1.50×10^{-1}	3.26×10^{-1}
k_{R6}	1.53×10^{9}	2.08×10^{9}	2.12×10^{9}	2.38×10^{9}	2.65×10^{9}
$k_{Total} = \sum_{i}^{7} k_{Ri}$	3.11×10^{12}	6.64×10^{12}	6.95×10^{12}	8.72×10^{12}	1.06×10^{13}

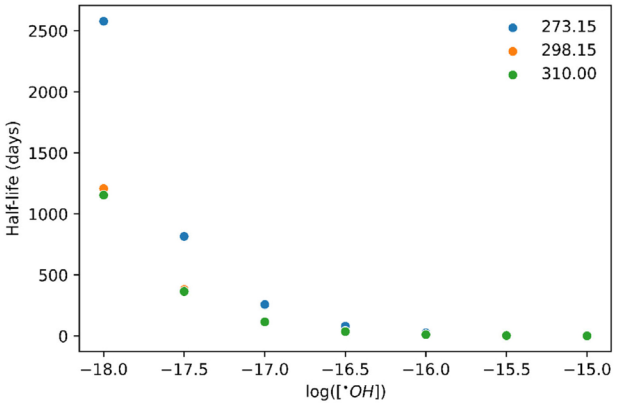

Figure 4. Half-life time, in days, of hydroxychloroquine degradation as a function of •OH concentration, in mol L^{-1}, in the temperature range 273.15-310 K of interest in natural waters.

acute toxicity (LC_{50} or EC_{50}) and chronic toxicity (ChV), respectively (see technical details in "Assessment of toxicity" sub-section).

The experimental cytotoxicity assay with mononuclear cell showed that the tizoxanide, the main degradation product (R5 channel), has a higher cytotoxicity when compared to NTZ with a reduction in cell viability of 75.25%, i.e., 27% higher than that obtained with NTZ in the concentration and tested conditions.[80] As can be seen in Table 4, the estimated toxicities of the compounds to fish, daphnia, and green algae showed that tizoxanide is more toxic than NTZ, in agreement with experimental results: it is attributed the harmful classification according to the European Union and Chinese Regulations.

The degradation of HCQ occurs by successive steps that lead to the formation of organic intermediates that end to mineralize. Here, we identified that R2 product is the most degradant product of neutral form of HQC. As can be seen in Table 5, the estimated toxicities of the compounds to fish, daphnia, and green algae showed that the R2 product is less toxic than HCQ.

Table 3. Classification of acute and chronic toxicity according to the criteria established by the European Union[86] and Chinese Regulations[87]

Classification	Acute toxicity[a]	Chronic toxicity[b]
Not harmful	$LC_{50} > 100$ or $EC_{50} > 100$	ChV > 10
Harmful	$10 < LC_{50} < 100$ or $10 < EC_{50} < 100$	1 < ChV < 10
Toxic	$1 < LC_{50} < 10$ or $1 < EC_{50} < 10$	0.1 < ChV < 1
Very toxic	$LC_{50} < 1$ or $EC_{50} < 1$	ChV < 0.1

[a]Criteria set by the European Union (described in Annex VI of Directive 67/548/EEC); [b]criteria set by the Chinese hazard evaluation guidelines for new chemical substances (HJ/T 154-2004). LC_{50}: acute toxicity; ChV: chronic toxicity.

Table 4. Toxicity of NTZ and its main by-product generated through •OH radical attack. The definition on Table 3 was used to classify the toxicity of compounds

Organism	Compound	
	NTZ	R5
LC_{50} (fish 96 h)	110	15.7[a]
LC_{50} (daphnia 48 h)	109	13.4[a]
EC_{50} (green algae 96 h)	12.7[a]	2.61
ChV (fish, chronic)	1.35[a]	0.03[b]
ChV (daphnia, chronic)	17.1	3.04[a]
ChV (green algae, chronic)	7.61[a]	2.44[a]

[a]Not harmful; [b]very toxic. LC_{50}: acute toxicity, ChV: chronic toxicity; NTZ: nitazoxanide; R5 the most kinetically favorable channel.

Table 5. Toxicity of HCQ and of its main by-product generated through •OH radical attack. The definition on Table 3 was used to classify the toxicity of compounds

Organism	Compound	
	HCQ	R2
LC_{50} (fish 96 h)	13.55[a]	85.66[a]
LC_{50} (daphnia 48 h)	1.82	10.03[a]
EC_{50} (green algae 96 h)	1.18	8.57
ChV (fish, chronic)	0.55	5.26[a]
ChV (daphnia, chronic)	0.17	0.81
ChV (green algae, chronic)	0.43	2.81[a]

[a]Harmful. LC_{50}: acute toxicity; ChV: chronic toxicity; HCQ: hydroxychloroquine; R2: the most kinetically favorable channel.

Conclusions

In the "Reaction rate theory" section, the parameters couple (E_0, d) and ($\bar{E}$, $\bar{d}$) were differentiated to avoid confusion. The former is related to molecular parameters at potential energy channel of the elementary step evaluated. The late is related with several contributions to the overall reaction rate constant. In both drugs, the energetic barriers E_0 and deformation parameters d for the most probable degradation product show apparent negative activation energy[47,85] and propensity to quantum tunneling effect.[88,89] These molecular phenomena guide the kinetic behavior to anti-Arrhenius and sub-Arrhenius behavior.[90,91] However, these reactions are diffusion-controlled processes which are typical cases of classical and cooperative effects mediated by the viscosity of the solvent in reactive molecular encounters.[91,92] Equations 4 and 5 capture the majority contribution of the solvent effect in reactive processes providing positive phenomenological parameters ($\bar{E}$, $\bar{d}$) with kinetic behavior befitting with super-Arrhenius cases, where transport phenomena, e.g., diffusion and viscosity, decelerate as the temperature decreases.

A theoretical study was performed on the degradation of nitazoxanide and hydroxychloroquine via •OH radicals in aqueous media using a combination of quantum chemistry calculations and reaction rate theories. The degradation mechanism and reaction kinetics were reported, and the results showed that deacetylation of nitazoxanide with formation of tizoxanide was the most kinetic favorable channel agreeing with experimental work. For hydroxychloroquine, the theoretical calculations showed that the addition •OH at carbon of aromatic ring (R2) was the most kinetic favorable channel. The reaction rate constants were calculated by formulations derived both from the Transition State Theory modified for quantum tunneling and from the theory of diffusion-controlled processes. The half-lives time for NTZ and HCQ degradation varied from 12 to 138 days. Both drugs presented toxicities between harmful and toxic. However, in the nitazoxanide degradation process, the R5 degradation compound was characterized as more toxic, while in the case of hydroxychloroquine the major degradation product, R2, showed a decrease in the toxicity.

Supplementary Information

Supplementary data are available free of charge at http://jbcs.sbq.org.br as PDF file.

Acknowledgments

The authors acknowledge the Brazilian funding agencies Coordenação de Aperfeiçoamento de Pessoal de Nível Superior (CAPES) and Conselho Nacional de Desenvolvimento Científico e Tecnológico (CNPq) for financial suport and CNPq Research Productivity Grant (314698/2021-3). Valter H. Carvalho-Silva thanks Goiana Agency (FAPEG) for the research funding programs (Auxílio à Pesquisa Colaborativa FAPEG-FAPESP/GSP2019011000037). This research is also supported by the High-Performance Computing Center at the Subsecretaria de Tecnologia da Informação (STI), in the Secretaria de Desenvolvimento e Inovação (SEDI), Brazil.

Author Contributions

All authors contributed to the study conception and design. Calculations, data collection and analysis were performed by Flávio O. Sanches-Neto, Nayara D. Coutinho and Valter H. Carvalho-Silva. The interpretation of data was performed by Flávio O. Sanches-Neto, Nayara D. Coutinho, Valter H. Carvalho-Silva, Vincenzo Aquilanti and Wender A. Silva. The first draft of the manuscript was written by Nayara D. Coutinho, and all authors commented on previous versions of the manuscript. All authors read and approved the final manuscript.

References

1. Mahase, E.; *BMJ* **2020**, *368*, m1166. [Crossref]
2. Hariyanto, T. I., Halim, D. A.; Jodhinata, C.; Yanto, T. A.; Kurniawan, A.; *Clin. Exp. Pharmacol. Physiol.* **2021**, *48*, 823. [Crossref]
3. Luo, Y.; Guo, W.; Hao, H.; Duc, L.; Ibney, F.; Zhang, J.; Liang, S.; Wang, X. C.; *Sci. Total Environ.* **2014**, *473-474*, 619. [Crossref]
4. López-Pacheco, I. Y.; Silva-Núñez, A.; Salinas-Salazar, C.; Arévalo-Gallegos, A.; Lizarazo-Holguin, L. A.; Barceló, D.; Iqbal, M. N.; Parra-Saldívar, R.; *Sci. Total Environ.* **2019**, *690*, 1068. [Crossref]
5. López-Doval, J. C.; Montagner, C. C.; Fernandes, A.; Alburquerque, D.; Moschini-Carlos, V.; Umbuzeiro, G.; Pompêo, M.; *Sci. Total Environ.* **2016**, *575*, 1307. [Crossref]
6. O'Flynn, D.; Lawler, J.; Yusuf, A.; Parle-Mcdermott, A.; Harold, D.; Mc Cloughlin, T.; Holland, L.; Regan, F.; White, B.; *Anal. Methods* **2021**, *13*, 575. [Crossref]
7. Rinaldo, A.; Rodriguez-Iturbe, I.; *Rend. Lincei Sci. Fis. Nat.* **2022**, *33*, 245. [Crossref]
8. Sharma, K.; Kaushik, G. In *Environmental Microbiology and Biotechnology*; Springer Singapore: Singapore, 2021, p. 267-292. [Crossref]
9. Ek, M.; Baresel, C.; Magnér, J.; Bergström, R.; Harding, M.; *Water Sci. Technol.* **2014**, *69*, 2372. [Crossref]

10. Khanzada, N. K.; Farid, M. U.; Kharraz, J. A.; Choi, J.; Tang, C. Y.; Nghiem, L. D.; Jang, A.; An, A. K.; *J. Membr. Sci.* **2020**, *598*, 117672. [Crossref]
11. Klavarioti, M.; Mantzavinos, D.; Kassinos, D.; *Environ. Int.* **2009**, *35*, 402. [Crossref]
12. Cuerda-Correa, E. M.; Alexandre-Franco, M. F.; Fernández-González, C.; *Water* **2019**, *12*, 102. [Crossref]
13. Sirés, I.; Brillas, E.; Oturan, M. A.; Rodrigo, M. A.; Panizza, M.; *Environ. Sci. Pollut. Res. Int*. **2014**, *21*, 8336. [Crossref]
14. Wang, J.; Zhuan, R.; *Sci. Total Environ.* **2020**, *701*, 135023. [Crossref]
15. Basturk, I.; Varank, G.; Murat-Hocaoglu, S.; Yazici-Guvenc, S.; Can-Güven, E.; Oktem-Olgun, E. E.; Canli, O.; *J. Environ. Chem. Eng.* **2021**, *9*, 104666. [Crossref]
16. Méndez-Arriaga, F.; Esplugas, S.; Giménez, J.; *Water Res.* **2010**, *44*, 589. [Crossref]
17. Madhavan, J.; Grieser, F.; Ashokkumar, M.; *J. Hazard. Mater. Lett.* **2010**, *178*, 202. [Crossref]
18. Saeid, S.; Tolvanen, P.; Kumar, N.; Eränen, K.; Peltonen, J.; Peurla, M.; Mikkola, J.-P.; Franz, A.; Salmi, T.; *Appl. Catal., B* **2018**, *230*, 77. [Crossref]
19. Keen, O. S.; Baik, S.; Linden, K. G.; Aga, D. S.; Love, N. G.; *Environ. Sci. Technol.* **2012**, *46*, 6222. [Crossref]
20. Kowalska, K.; Maniakova, G.; Carotenuto, M.; Sacco, O.; Vaiano, V.; Lofrano, G.; Rizzo, L.; *Chemosphere* **2020**, *238*, 124665. [Crossref]
21. Monteoliva-García, A.; Martín-Pascual, J.; Muñío, M. M.; Poyatos, J. M.; *Int. J. Environ. Sci. Technol.* **2019**, *16*, 6005. [Crossref]
22. Souza, F. S.; da Silva, V. V.; Rosin, C. K.; Hainzenreder, L.; Arenzon, A.; Féris, L. A.; *Environ. Technol.* **2018**, *39*, 549. [Crossref]
23. de Carvalho, J. F.; de Moraes, J. E. F.; *Environ. Technol* **2020**, *42*, 4145. [Crossref]
24. Ay, F.; Kargi, F.; *J. Hazard. Mater.* **2010**, *179*, 622. [Crossref]
25. González, O.; Sans, C.; Esplugas, S.; Malato, S.; *Photochem. Photobiol. Sci.* **2009**, *8*, 1032. [Crossref]
26. Martini, J.; Orge, C. A.; Faria, J. L.; Pereira, M. F. R.; Soares, O. S. G. P.; *J. Environ. Chem. Eng.* **2018**, *6*, 4054. [Crossref]
27. Martini, J.; Orge, C. A.; Faria, J. L.; Pereira, M. F. R.; Soares, O. S. G. P.; *Appl. Sci.* **2019**, *9*, 2652. [Crossref]
28. Du, L.; Xu, W.; Liu, Y.; Li, X.; Huang, D.; Wu, S.; *Water, Air, Soil Pollut.* **2020**, *231*, 159. [Crossref]
29. Sirés, I.; Arias, C.; Cabot, P. L.; Centellas, F.; Rodríguez, R. M.; Garrido, J. A.; Brillas, E.; *Environ. Chem.* **2004**, *1*, 26. [Crossref]
30. Torun, M.; Gültekin, Ö.; Şolpan, D.; Güven, O.; *Environ. Technol.* **2015**, *36*, 970. [Crossref]
31. Audino, F.; Toro Santamaria, J.; del Valle Mendoza, L.; Graells, M.; Pérez-Moya, M.; *Int. J. Environ. Res. Public Health* **2019**, *16*, 505. [Crossref]
32. Manonmani, G.; Sandhiya, L.; Senthilkumar, K.; *J. Phys. Chem. A* **2019**, *123*, 8954. [Crossref]
33. Manonmani, G.; Sandhiya, L.; Senthilkumar, K.; *Environ. Sci. Pollut. Res.* **2020**, *27*, 12080. [Crossref]
34. Mei, Q.; Sun, J.; Han, D.; Wei, B.; An, Z.; Wang, X.; Xie, J.; Zhan, J.; He, M.; *Chem. Eng. J.* **2019**, *373*, 668. [Crossref]
35. An, T.; Gao, Y.; Li, G.; Kamat, P. V.; Peller, J.; Joyce, M. V.; *Environ. Sci. Technol.* **2014**, *48*, 641. [Crossref]
36. Milenković, D. A.; Dimić, D. S.; Avdović, E. H.; Amić, A. D.; Dimitrić Marković, J. M.; Marković, Z. S.; *Chem. Eng. J.* **2020**, *395*, 124971. [Crossref]
37. Xiao, R.; Ma, J.; Luo, Z.; Zeng, W.; Wei, Z.; Spinney, R.; Hu, W.; Dionysiou, D. D.; *Environ. Pollut.* **2020**, *257*, 113498. [Crossref]
38. Sanches-Neto, F. O.; Ramos, B.; Lastre-Acosta, A. M.; Teixeira, A. C. S. C.; Carvalho-Silva, V. H.; *Chemosphere* **2021**, *278*, 130401. [Crossref]
39. Yang, Z.; Su, R.; Luo, S.; Spinney, R.; Cai, M.; Xiao, R.; Wei, Z.; *Sci. Total Environ.* **2017**, *590-591*, 751. [Crossref]
40. Wang, P.; Bu, L.; Wu, Y.; Ma, W.; Zhu, S.; Zhou, S.; *Chemosphere* **2021**, *267*, 128883. [Crossref]
41. Hammond, J.; Leister-Tebbe, H.; Annie, G.; Abreu, P.; Weihang, B.; Wayne, W.; MaryLynn, B.; Hendrick, V.; Damle, B.; Simón-Campos Abraham, Pypstra, R.; Rusnak, J. M.; *N. Engl. J. Med.* **2022**, *386*, 1397. [Crossref]
42. Jayk Bernal, A.; Gomes da Silva, M. M.; Musungaie, D. B.; Kovalchuk, E.; Gonzalez, A.; Delos Reyes, V.; Martín-Quirós, A.; Caraco, Y.; Williams-Diaz, A.; Brown, M. L.; Du, J.; Pedley, A.; Assaid, C.; Strizki, J.; Grobler, J. A.; Shamsuddin, H. H.; Tipping, R.; Wan, H.; Paschke, A.; Butterton, J. R.; Johnson, M. G.; de Anda, C.; *N. Engl. J. Med.* **2022**, *386*, 509. [Crossref]
43. Tarighi, P.; Eftekhari, S.; Chizari, M.; Sabernavaei, M.; Jafari, D.; Mirzabeigi, P.; *Eur. J. Pharmacol.* **2021**, *895*, 173890. [Crossref]
44. Mahase, E.; *BMJ* **2020**, *368*, 1. [Crossref]
45. Rossignol, J.-F.; *Antiviral Res.* **2014**, *110*, 94. [Crossref]
46. Rocco, P. R. M.; Silva, P. L.; Cruz, F. F.; Junior, M. A. C. M.; Tierno, P. F. G. M. M.; Moura, M. A.; De Oliveira, L. F. G.; Lima, C. C.; Dos Santos, E. A.; Junior, W. F.; Fernandes, A. P. S. M.; Franchini, K. G.; Magri, E.; de Moraes, N. F.; Gonçalves, J. M. J.; Carbonieri, M. N.; dos Santos, I. S.; Paes, N. F.; Maciel, P. V. M.; Rocha, R. P.; de Carvalho, A. F.; Alves, P. A.; Modena, J. L. P.; Cordeiro, A. T.; Trivella, D. B. B.; Marques, R. E.; Luiz, R. R.; Pelosi, P.; Lapa e Silva, J. R.; *Eur. Respir. J.* **2020**, 2003725. [Crossref]
47. Malesuik, M. D.; Gonçalves, H. M. L.; Garcia, C. V.; Trein, M. R.; Nardi, N. B.; Schapoval, E. E. S.; Steppe, M.; *Talanta* **2012**, *93*, 206. [Crossref]
48. Ben-Zvi, I.; Kivity, S.; Langevitz, P.; Shoenfeld, Y.; *Clin. Rev. Allergy Immunol.* **2012**, *42*, 145. [Crossref]

49. Al-Bari, M. A. A.; *J. Antimicrob. Chemother.* **2015**, *70*, 1608. [Crossref]
50. Howard, B. In *xPharm: The Comprehensive Pharmacology Reference*; Elsevier: Amsterdam, 2007, p. 1-4. [Crossref]
51. Gasmi, A.; Peana, M.; Noor, S.; Lysiuk, R.; Menzel, A.; Gasmi Benahmed, A.; Bjørklund, G.; *Appl. Microbiol. Biotechnol.* **2021**, *105*, 1333. [Crossref]
52. Kumar, R.; Sharma, A.; Srivastava, J. K.; Siddiqui, M. H.; Uddin, M. S.; Aleya, L.; *Environ. Sci. Pollut. Res.* **2021**, *28*, 40431. [Crossref]
53. Elavarasi, A.; Prasad, M.; Seth, T.; Sahoo, R. K.; Madan, K.; Nischal, N.; Soneja, M.; Sharma, A.; Maulik, S. K.; Shalimar; Garg, P.; *J. Gen. Intern. Med.* **2020**, *35*, 3308. [Crossref]
54. Saini, B.; Bansal, G.; *J. Pharm. Biomed. Anal.* **2013**, *84*, 224. [Crossref]
55. Dabić, D.; Babić, S.; Škorić, I.; *Chemosphere* **2019**, *230*, 268. [Crossref]
56. Bensalah, N.; Midassi, S.; Ahmad, M. I.; Bedoui, A.; *Chem. Eng. J.* **2020**, *402*, 126279. [Crossref]
57. Han, D.; Li, J.; Cao, H.; He, M.; Hu, J.; Yao, S.; *Chemosphere* **2014**, *95*, 50. [Crossref]
58. López, P.; Méndez, F.; *Org. Lett.* **2004**, *6*, 1781. [Crossref]
59. Melin, J.; Ayers, P. W.; Ortiz, J. V.; *J. Phys. Chem. A* **2007**, *111*, 10017. [Crossref]
60. Lu, T.; Chen, F.; *J. Comput. Chem.* **2012**, *33*, 580. [Crossref]
61. Frisch, M. J.; Trucks, G. W.; Schlegel, H. B.; Scuseria, G. E.; Robb, M. A.; Cheeseman, J. R.; Scalmani, G.; Barone, V.; Petersson, G. A.; Nakatsuji, H.; Li, X.; Caricato, M.; Marenich, A. V; Bloino, J.; Janesko, B. G.; Gomperts, R.; Mennucci, B.; Hratchian, H. P.; Ortiz, J. V; Izmaylov, A. F.; Sonnenberg, J. L.; Williams-Young, D.; Ding, F.; Lipparini, F.; Egidi, F.; Goings, J.; Peng, B.; Petrone, A.; Henderson, T.; Ranasinghe, D.; Zakrzewski, V. G.; Gao, J.; Rega, N.; Zheng, G.; Liang, W.; Hada, M.; Ehara, M.; Toyota, K.; Fukuda, R.; Hasegawa, J.; Ishida, M.; Nakajima, T.; Honda, Y.; Kitao, O.; Nakai, H.; Vreven, T.; Throssell, K.; Montgomery Jr., J. A.; Peralta, J. E.; Ogliaro, F.; Bearpark, M. J.; Heyd, J. J.; Brothers, E. N.; Kudin, K. N.; Staroverov, V. N.; Keith, T. A.; Kobayashi, R.; Normand, J.; Raghavachari, K.; Rendell, A. P.; Burant, J. C.; Iyengar, S. S.; Tomasi, J.; Cossi, M.; Millam, J. M.; Klene, M.; Adamo, C.; Cammi, R.; Ochterski, J. W.; Martin, R. L.; Morokuma, K.; Farkas, O.; Foresman, J. B.; Fox, D. J.; *Gaussian16 Revision C.01*, Gaussian Inc., Wallingford CT, 2016.
62. Marenich, A. V.; Cramer, C. J.; Truhlar, D. G.; *J. Phys. Chem. B* **2009**, *113*, 6378. [Crossref]
63. Carvalho-Silva, V. H.; Aquilanti, V.; de Oliveira, H. C. B.; Mundim, K. C.; *J. Comput. Chem.* **2017**, *38*, 178. [Crossref]
64. Collins, F. C.; Kimball, G. E.; *Ind. Eng. Chem.* **1949**, *41*, 2551. [Crossref]
65. Sanches-Neto, F. O.; Coutinho, N. D.; Palazzetti, F.; Carvalho-Silva, V. H.; *Struct. Chem.* **2020**, *31*, 609. [Crossref]
66. Aquilanti, V.; Mundim, K. C.; Elango, M.; Kleijn, S.; Kasai, T.; *Chem. Phys. Lett.* **2010**, *498*, 209. [Crossref]
67. Machado, H. G.; Sanches-Neto, F. O.; Coutinho, N. D.; Mundim, K. C.; Palazzetti, F.; Carvalho-Silva, V. H.; *Molecules* **2019**, *24*, 3478. [Crossref]
68. Mphyschem, www.mphyschem.com/transitivity, accessed in January 2023.
69. *ECOSAR*, v2.0; U.S. EPA, Washington, USA, 2017. [Link] accessed in January 2023
70. Sanderson, H.; Johnson, D. J.; Wilson, C. J.; Brain, R. A.; Solomon, K. R.; *Toxicol. Lett.* **2003**, *144*, 383. [Crossref]
71. Reuschenbach, P.; Silvani, M.; Dammann, M.; Warnecke, D.; Knacker, T.; *Chemosphere* **2008**, *71*, 1986. [Crossref]
72. Silva, V. H. C.; Camargo, L.; Napolitano, H. B.; Pérez, C. N.; Camargo, A. J.; *J. Mol. Graphics Modell.* **2010**, *29*, 206. [Crossref]
73. Timonen, R. S.; Seetula, J. A.; Gutman, D.; *J. Chem. Inf. Model.* **1990**, *94*, 3005. [Crossref]
74. Seetula, J. A.; *J. Chem. Soc., Faraday Trans.* **1998**, *94*, 891. [Crossref]
75. Jaramillo, V. I.; Gougeon, S.; Le Picard, S. D. S. D.; Canosa, A. A.; Smith, M. A.; Rowe, B. R.; *Int. J. Chem. Kinet.* **2002**, *34*, 339. [Crossref]
76. Stone, D.; Rowley, D. M.; *Phys. Chem. Chem. Phys.* **2005**, *7*, 2156. [Crossref]
77. Campuzano-Jost, P.; Crowley, J. N.; *J. Phys. Chem. A* **1999**, *103*, 2712. [Crossref]
78. Coutinho, N. D.; Silva, V. H. C.; de Oliveira, H. C. B.; Camargo, A. J.; Mundim, K. C.; Aquilanti, V.; *J. Phys. Chem. Lett.* **2015**, *6*, 1553. [Crossref]
79. Coutinho, N. D.; Aquilanti, V.; Silva, V. H. C.; Camargo, A. J.; Mundim, K. C.; de Oliveira, H. C. B.; *J. Phys. Chem. A* **2016**, *120*, 5408. [Crossref]
80. Sudhakaran, S.; Amy, G. L.; *Water Res.* **2013**, *47*, 1111. [Crossref]
81. de Souza, L. P.; Sanches-Neto, F. O.; Yuki Jr., G. M.; Ramos, B.; Lastre-Acosta, A. M.; Carvalho-Silva, V. H.; Teixeira, A. C. S. C.; *Process Saf. Environ. Prot.* **2022**, *166*, 478. [Crossref]
82. PYSIRC, www.pysirc.com.br, accessed in January 2023.
83. Brezonik, P. L.; Fulkerson-Brekken, J.; *Environ. Sci. Technol.* **1998**, *32*, 3004. [Crossref]
84. Yang, J.; Wang, Z.; Lv, G.; Liu, W.; Wang, Y.; Sun, X.; Gao, J.; *Ecotoxicol. Environ. Saf.* **2020**, *197*, 110644. [Crossref]
85. Burns, J. M.; Cooper, W. J.; Ferry, J. L.; King, D. W.; DiMento, B. P.; McNeill, K.; Miller, C. J.; Miller, W. L.; Peake, B. M.; Rusak, S. A.; Pοσε, Λ. A.; Waite, T. D.; *Aquat. Sci.* **2012**, *74*, 683. [Crossref]
86. Commission of the European Communities; *Annex VI of Directive 67/548/EEC, General Classification and Labelling Requirements for Dangerous Substances and Preparation*,

vol. 225; Official Journal of the European Union, 2001. [Link] accessed in February 2023
87. Chinese Hazard Evaluation; *HJ/T 154-2004: The Guidelines for the Hazard Evaluation of New Chemical Substances*, 2004. [Link] accessed in February 2023
88. Coutinho, N. D.; Sanches-Neto, F. O.; Carvalho-Silva, V. H.; de Oliveira, H. C. B.; Ribeiro, L. A.; Aquilanti, V.; *J. Comput. Chem.* **2018**, *39*, 2508. [Crossref]
89. Sanches-Neto, F. O.; Coutinho, N. D.; Carvalho-Silva, V. H.; *Phys. Chem. Chem. Phys.* **2017**, *19*, 24467. [Crossref]
90. Carvalho-Silva, V. H.; Coutinho, N. D.; Aquilanti, V.; *Molecules* **2020**, *25*, 2098. [Crossref]
91. Carvalho-Silva, V. H.; Coutinho, N. D.; Aquilanti, V.; *Front. Chem.* **2019**, *7*, 380. [Crossref]
92. Aquilanti, V.; Coutinho, N. D.; Carvalho-Silva, V. H.; *Philos. Trans. R. Soc., A* **2017**, *375*, 20160201. [Crossref]

Submitted: September 2, 2022
Published online: February 24, 2023